ACS SENSORS

pubs.acs.org/acssensors

Article

MXene Enhanced Photoactivity of Bi_2O_3/Bi_2S_3 Heterojunction with G-wire Superstructure for Photoelectrochemical Detection of TET1 Protein

Yulin Zheng, Xiaoting Cui, Yunlei Zhou,* Haowei Zhang, Lulu Cao, Lanlan Gao, Huanshun Yin,* and Shiyun Ai

Cite This: *ACS Sens.* 2022, 7, 3116−3125

Read Online

ACCESS | Metrics & More | Article Recommendations | Supporting Information

ABSTRACT: Ten-eleven translocation 1 (TET1) protein has the potential to accelerate the oxygenation of 5-methylcytosine to 5-hydroxymethylcytosine (5hmC); then the $-CH_2OH$ of 5hmC can further covalently react with −SH catalyzed by M.*Hha*I methyltransferase. A brand-new photoelectrochemical (PEC) detection technique for the TET1 protein was created in light of this. For this objective, the Bi_2O_3/Bi_2S_3 heterojunction was first prepared by a one-pot hydrothermal method and served for photosensitive materials. For further enhancing the photoactivity, Bi_2O_3/Bi_2S_3 was blended with MXene to form an energy band-matched structure, thus improving the migration kinetics of photogenerated carriers. For achieving a high sensitivity of detection, a DNA Walker incorporated with the nicking endonuclease (Nb.BbvCI enzyme)-assisted signal amplification strategy was presented to output exponential G-quadruplex fragments. Self-assembly of the free G-quadruplex sequence into a G-wire superstructure with the assistance of Mg^{2+} provided more loading sites for MB and amplified the PEC signal. The linear range of the biosensor was 0.1−10 μg/mL with a detection limit of 0.024 μg/mL (S/N = 3) for TET1 protein under optimal experimental conditions. The suitability of the proposed method was evaluated by inhibitor screening experiments and the influence of environmental degradation on the activity of TET1 protein.

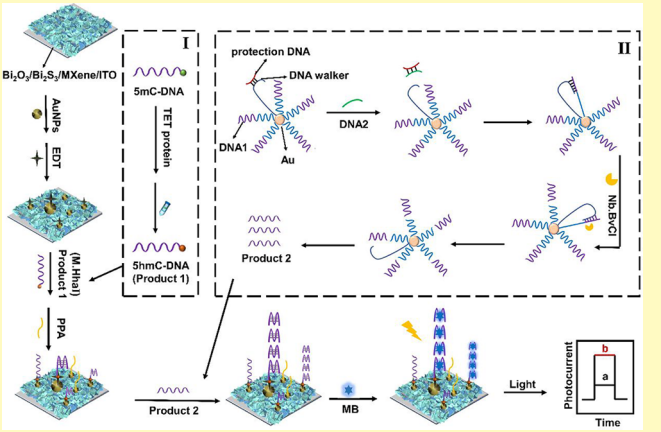

KEYWORDS: *Photoelectrochemical biosensor, MXene, DNA Walker, G-wire superstructure, TET1 protein, Perfluorinated compound, Inhinbitor, Ecotoxicological effects of pollutants*

DNA methylation is one of the most typical epigenetic modifications and plays an important role in embryonic development, cell differentiation, genetic imprinting, and regulation of gene expression.[1,2] The ten-eleven translocation 1 (TET1) protein is involved in DNA demethylation through iterative oxidation of 5-methylcytosine (5mC) to form 5-hydroxymethylcytosine (5hmC), 5-formylcytosine (5fC), and 5-carboxycytosine (5caC).[3−5] It has been found that the TET1 protein is widely present in a variety of cells, which affects the migration, proliferation, and invasion of many types of cancer cells.[6] The levels of TET1 protein usually change significantly with tumorigenesis, and the detection of the changes in its levels can be used to predict disease onset, suggesting that TET1 protein is expected to be a new marker for disease diagnosis and detection.[7,8] However, the functional study of the TET1 protein is still unclear, and establishing a facile and selective approach to study the function of TET1 protein is essential.

Currently, to better understand the role of TET1 protein in gene regulation, researchers have attempted to assess TET1 activity using classic thin-layer chromatography (TLC) and 2D-TLC,[9] fluorescence assay,[10] liquid chromatography−mass spectrometry (LC-MS),[11] electrochemiluminescence,[12] and TET1 activity/inhibition Assay Kit. However, most of these methods are usually limited by the disadvantages of cumbersome steps, large sample volumes, expensive instruments, and long assay time. Therefore, it is urgent to establish a facile economical and accurate method for TET1 detection. Photoelectrochemical (PEC) technology is a promising

Received: July 25, 2022
Accepted: September 29, 2022
Published: October 7, 2022

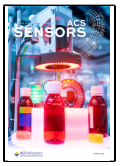

analysis technique with separated signal generation and signal output. In fact, light was employed to excite the photoactive nanomaterial to generate electrochemical signal. With the advantages of independent light source and detection signal device, low background signal, high sensitivity, low cost, and ease of operation, the PEC technique has been widely used in the field of biosensors for the detection of various biomolecules, including DNA,[13] RNA,[14] and proteins,[15] indicating that PEC analysis should be an ideal platform for TET1 protein detection.

In general, two key components are required to realize a sensitive PEC sensing system: the photosensitive materials and an amplified signal unit.[16] Particularly, the fabrication of materials is regarded as one of the key steps for designing highly sensitive PEC sensors. Bismuth-based compounds have been widely used in solar cells, gas sensors, supercapacitors, and batteries.[17,18] Among various bismuth-based compounds, bismuth oxides and bismuth sulfides are commonly found in the earth's crust and have been found to have various applications.[17] Among them, Bi_2O_3 is of great interest due to its high dielectric constant, low toxicity, and remarkable photoconductivity.[19,20] Nonetheless, the photogenerated electron−hole pair's rapid compounding limits the application of Bi_2O_3. To improve the photoelectric properties of Bi_2O_3, heterojunctions are constructed by combining Bi_2O_3 with other semiconductor materials with narrower band gaps. The optoelectronic properties of Bi_2O_3 can be improved.[21]

Among many semiconductors, Bi_2S_3 was recognized as an essential narrow band gap semiconductor,[22] with good stability[23] and diverse structural morphology, and can suppress the recombination of electron−hole (e^-/h^+) pairs and is an excellent material for prolonging visible light absorption, improving the charge transport performance of light generation.[24] In addition, Bi_2S_3 can easily form heterostructures with Bi_2O_3 due to its suitable energy band structure, which will produce energy band bending at the Bi_2O_3/Bi_2S_3 heterostructure interface, leading to carrier redistribution at the heterostructure interface and surface, and improving significantly the photoinduced carrier transport efficiency.[25] Based on these superb properties, a number of specialists have made remarkable achievements in the field of photocatalysis. For instance, Chen et al. prepared dendritic Bi_2O_3@Bi_2S_3 photocatalysts by etching and regeneration methods.[20] Sang et al. synthesized nanoflower-like Bi_2O_3/Bi_2S_3 heterojunctions by a one-pot method.[25] Based on the above advantages, the rational use of Bi_2O_3/Bi_2S_3 composites for the preparation of PEC biosensors will have great potential in the field of biosensing. However, the visible light activity of Bi_2O_3/Bi_2S_3 is limited and inhibits the PEC response of Bi_2O_3/Bi_2S_3. To improve its PEC response, the construction of energy−energy band-matched structures with other nanomaterials containing full-spectrum adsorption ability is an effective strategy.

MXene, as a noble metal-free material, has attracted much attention in various electrochemical applications such as supercapacitors,[26] batteries,[27] and electrocatalysis.[28,29] With strong full-spectrum absorption, good hydrophilicity, and excellent carrier migration and rich physical groups, two-dimensional MXenes were promising for applications in PEC research.[30] Primitive MXenes have metallic properties and abundant functional groups, which can be tightly bonded with *n*-type semiconductors to form energy band matching structures.[31] At the semiconductor/metal interface, photogenerated electrons from semiconductors will migrate from semiconductors to MXene, and the unique layer-like structure of MXene can effectively enhance the separation of photogenerated electrons and holes.[32] So far, a large number of Ti_3C_2-based heterostructured photocatalysts have been investigated, such as $BaSnO_3$/MXene,[33] PtO@Ti_3C_2/TiO_2,[34] $NiFe_2O_4$/MXene,[35] CuO/MXene,[36] etc.

In addition to excellent photoactive materials, the signal amplification unit is also an important factor affecting the detection sensitivity.[16] To meet the needs of detection with high sensitivity, advanced approaches to signal amplification of various kinds have become available methods, such as enzyme-catalyzed in situ precipitation,[37] in situ generation of electron donor,[38−40] dye sensitization,[41] and in situ formation of optically active substances.[42] Dye sensitization has the strengths of extensive absorption, efficient light absorption, and unique electronic structure, making it an attractive signal amplification strategy. Methylene blue (MB), a low-toxicity small organic molecule dye among various types of dyes, accelerates the transmission of electrons across the helix structure and enhances the electrical properties of DNA.[43] In addition, MB has a strong attraction to the negatively charged phosphate skeleton and can be electrostatically attraction to the G-wire. Due to the advantages of the $\pi-\pi$ conjugated electron structure, high-speed electron injection kinetics, remarkable visible absorbing performance, and inexpensive cost, it has been widely used in optoelectronic biosensors.[44]

In this paper, a unique and sensitive PEC biosensor for the detection of TET1 protein with multiple signal amplification was investigated. Bi_2O_3/Bi_2S_3 nanoflowers were prepared with a one-pot coprecipitation method and were used as the photoactive material. MXene was employed to improve the PEC activity of Bi_2O_3/Bi_2S_3, G-wire served as the signal amplification unit, and MB was adopted as the photosensitizer. By taking the catalytic activity of the TET1 protein for oxidation of 5mC to produce 5hmC and combining with the covalent reaction between $-CH_2OH$ of 5hmC and $-SH$ under the catalysis of M.*Hha*I methyltransferase, a sensitive PEC method was developed for detection of TET1 protein. First, Bi_2O_3/Bi_2S_3 nanoflowers and MXene and Au nanoparticle layers were sequentially modified on the electrode surface. Using the M.*Hha*I methyltransferase-catalyzed reaction between $-SH$ and $-CH_2OH$ as a specific recognition method, short sequence DNA containing 5hmC base (5hmC-DNA) was immobilized on the electrode surface to form a G-quadruplex in the presence of K^+.[45] In addition, after DNA Walker (DW) was released from the duplex of protected DNA (PD), it could be used with DNA1 having a cleavage endonuclease (Nb.BbvCI)-specific cleavage site hybridization, after which DNA1 was cleaved specifically by the Nb.BbvCI enzyme, resulting in a large amount of product.[46] The obtained electrodes were then incubated with the products and further superimposed in the presence of K^+ and Mg^{2+} to form the G-wire superstructure.[16,47] Subsequently, a large amount of MB can be inserted into the G-quadruplex to achieve effective sensitization to MXene/Bi_2O_3/Bi_2S_3, resulting in a significantly increased photocurrent signal for quantitative analysis of TET1 protein. The effects of perfluorinated compounds on TET1 protein activity were investigated using this method. Furthermore, the viability of the TET1 protein for the evaluation of ecotoxicological and toxicological effects of environmental pollutants as a biomarker was analyzed.

https://doi.org/10.1021/acssensors.2c01600
ACS Sens. 2022, 7, 3116−3125

Scheme 1. Schematic Illustration of the Preparation of MXene and Bi_2O_3/Bi_2S_3 (A), PEC Biosensor Construction (B), and the Influence of Environmental Pollutant on TET1 Protein Activity (C)

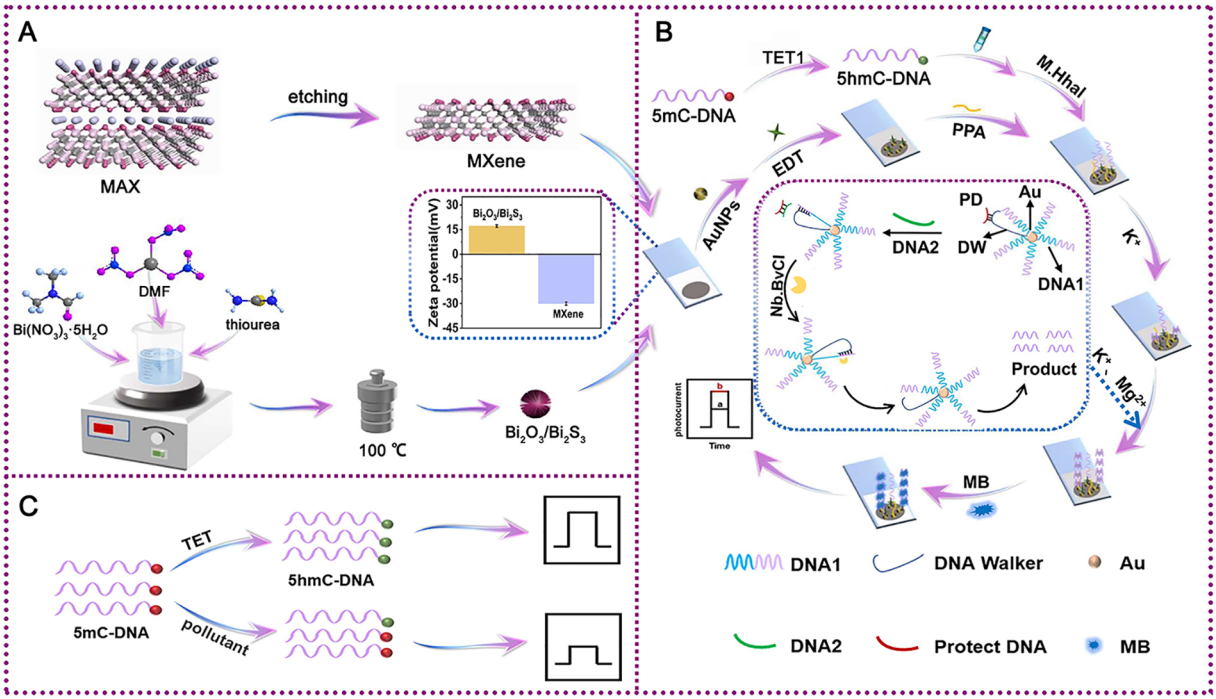

EXPERIMENTAL SECTION

See Supporting Information.

RESULTS AND DISCUSSION

Detection Principle. With the combination of the MXene and Bi_2O_3/Bi_2S_3 photosensitive material system and the DNA Walker and G-wire signal amplification techniques, a highly selective and sensitive antibody-free PEC biosensor for the detection of TET1 protein was established. The preparation procedure of the photoactive materials was illustrated in Scheme 1A. Due to the matched energy band potential between Bi_2O_3, Bi_2S_3, and MXene, and the full visible light activity of Bi_2S_3 and MXene, the PEC response of Bi_2O_3 was improved greatly under visible light excitation. The zeta potentials of Bi_2O_3/Bi_2S_3 nanoflowers and MXene were tested to be 17.19 ± 0.77 mV and −30.01 ± 0.99 mV, respectively. By electrostatic attachment both materials can be combined simultaneously (Scheme 1A). Scheme 1B presented the preparation procedure of the biosensor and TET1 protein detection strategy. Upon the immobilization of Bi_2O_3/Bi_2S_3, MXene, and AuNPs on the pretreated ITO electrode, the EDT was further trapped according to the Au−S bond formation. EDT possessed two sulfhydryl; one reacted with Au to form Au−S bond for EDT immobilization, and the other sulfhydryl group was left on, and distant from the electrode surface, it served as a trapping agent for 5hmC-DNA. Subsequently, the AuNPs surface was blocked by propylamine to eliminate the nonspecific adsorption. By taking advantage of the oxidation activity of TET1 protein toward 5mC to produce 5hmC, 5hmC-DNA was obtained with its target sequence as an assignment for the indirect test for the activity of the TET1 protein. To eliminate the possible interference from the TET protein, the 5hmC-DNA was purified by ultrafiltration. Subsequently, based on the specific covalent reaction between the $-CH_2OH$ of 5hmC and −SH of EDT catalyzed by the M.*Hha*I methyltransferase, 5hmC-DNA was specifically recognized and captured on the electrode surface. In the presence of K^+, 5hmC-DNA changed its single-stranded structure to a G-quadruplex structure by $\pi-\pi$ superposition with the assistance of K^+, triggering the future assembly of G-quadruplex to form a long filamentous G-wire structure. As seen in the inset of Scheme 1B, after DNA Walker (DW) and DNA1 bind with AuNPs to form the DNA-AuNPs composite, the fragment of DW DNA hybridized with PD DNA, blocking the hybridization between DW DNA and DNA1. However, the hybridization between PD DNA and DW DNA was blocked when DNA2 was introduced with the system. That is, DNA2 hybridized with PD DNA, leading to the release of DW DNA. Subsequently, DW DNA was further hybridized with DNA1, triggering the digestion activity of the Nb.BvCI nicking enzyme, resulting in a large amount of product of single-strand DNA (Light purple) as amplification signal DNA. These DNA was then incubated onto the electrode surface in the presence of K^+ and Mg^{2+}, leading to the stacking of G-quadruplex to form a long filamentous G-wire structure. Ultimately, as a signal amplification molecule, MB was captured by the G-quadruplex through $\pi-\pi$ superposition and electrostatic interactions, which further amplify the PEC response. Based on the linear relationship between the PEC response and TET1 protein concentration, quantitative detection of TET1 protein was achieved.

For evaluating the applicability of the approach, the inhibitor screening and the effect of environmental pollutant on TET1 protein were performed. Using Bobcat339 as a model inhibitor and perfluorohexanesulfonate as a topical environmental pollutant, the effect of Bobcat339 and perfluorohexanesulfonate on TET1 protein activity was investigated.

Characterization of Materials. The structures and shapes of Bi_2O_3, Bi_2S_3, and Bi_2O_3/Bi_2S_3 through SEM have been observed. This is a lamellar aggregation of the irregular

https://doi.org/10.1021/acssensors.2c01600
ACS Sens. 2022, 7, 3116−3125

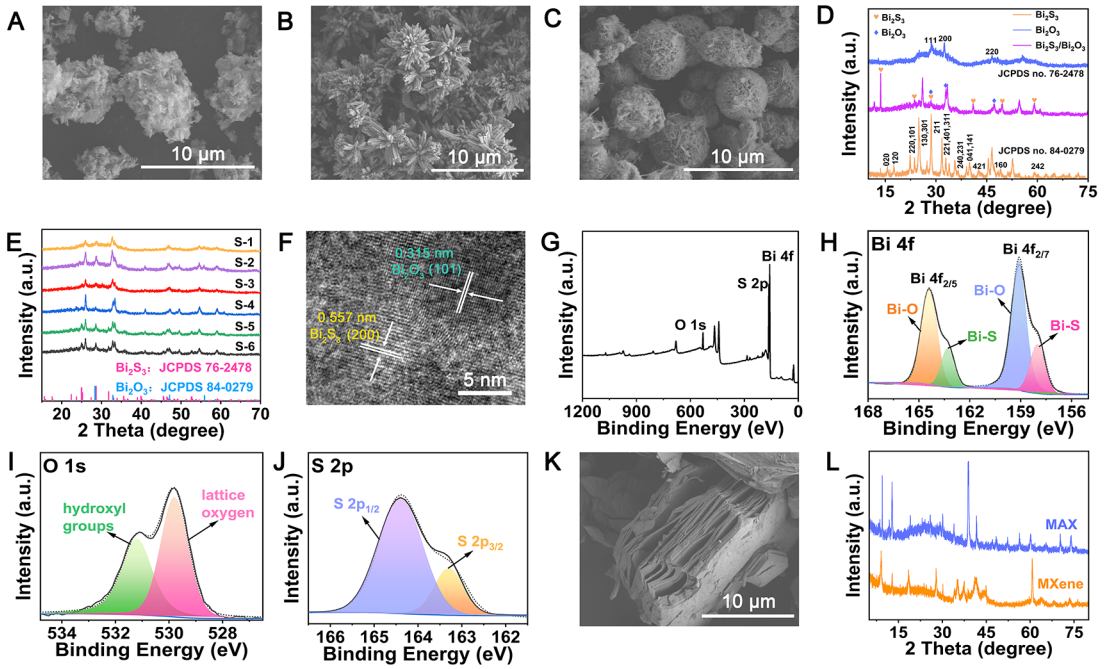

Figure 1. SEM images of Bi_2O_3 (A), Bi_2S_3 (B), Bi_2O_3/Bi_2S_3 (C), and MXene (K). XRD patterns of Bi_2O_3, Bi_2S_3 and Bi_2O_3/Bi_2S_3 (S-4) (D), Bi_2O_3/Bi_2S_3 heterojunctions (S-1−S-6) (E), and MXene (L). HR-TEM image of Bi_2O_3/Bi_2S_3 (S-4) (F). XPS patterns of Bi_2O_3/Bi_2S_3 (S-4) heterojunction: (G) Bi 4f spectrum (H), O 1s spectrum (I), and S 2p spectrum (J).

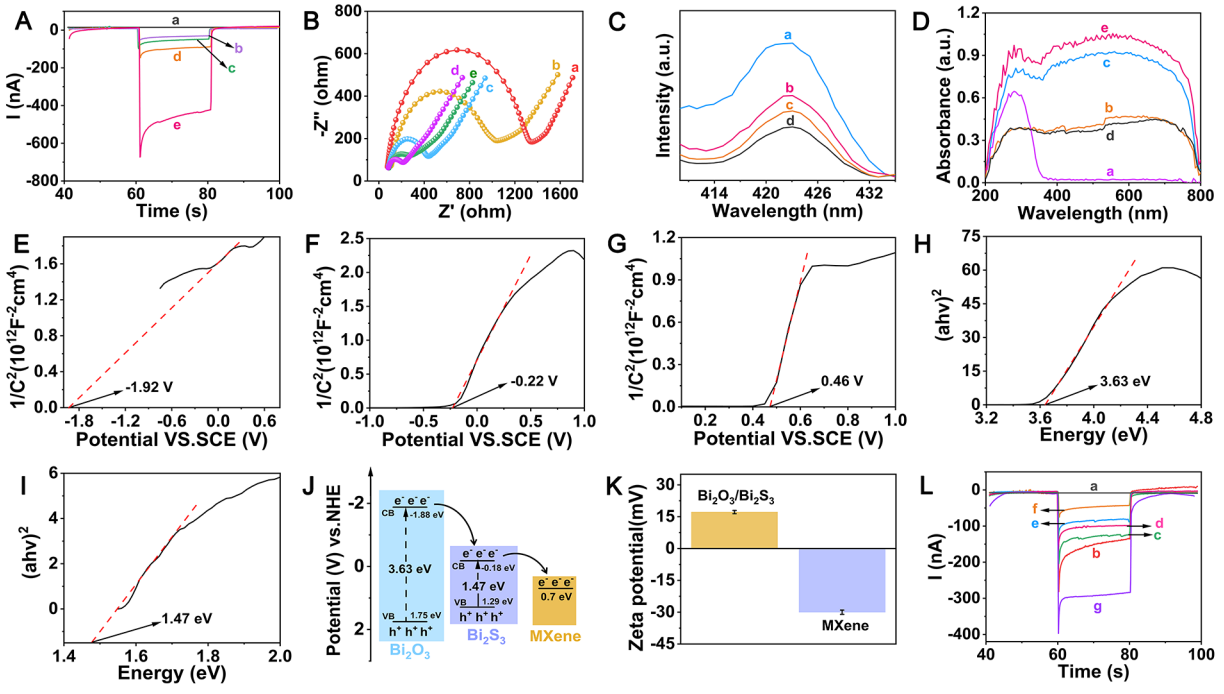

Figure 2. (A) PEC response of different electrodes in 0.1 M Tris-HCl and 0.1 M MB (pH 7.4). (a) MXene/ITO, (b) Bi_2O_3/ITO, (c) Bi_2S_3/ITO, (d) Bi_2O_3/Bi_2S_3/ITO, and (e) MXene/Bi_2O_3/Bi_2S_3/ITO. (B) Nyquist plot of Bi_2O_3/ITO (a), Bi_2S_3/ITO (b), Bi_2O_3/Bi_2S_3/ITO (c), MXene/ITO (d), and MXene/Bi_2O_3/Bi_2S_3/ITO (e) in 5 mM $Fe(CN)_6^{3-/4-}$ and 0.1 M KCl. (C) PL spectra of Bi_2O_3 (a), Bi_2S_3 (b), Bi_2O_3/Bi_2S_3 (c), and MXene/Bi_2O_3/Bi_2S_3 (d). (D) UV−vis DRS spectra of Bi_2O_3 (a), Bi_2S_3 (b), Bi_2O_3/Bi_2S_3 (c), MXene (d), and MXene/Bi_2O_3/Bi_2S_3 (e). Mott−Schottky plot of Bi_2O_3 (E), Bi_2S_3 (F), and MXene (G). UV−vis DRS of Bi_2O_3 (H) and Bi_2S_3 (I). (J) Possible mechanism for enhanced photoactivity. (K) Zeta potential of MXene and Bi_2O_3/Bi_2S_3. (L) PEC response of different electrodes in 0.1 M Tris-HCl (pH = 7.4). (a) ITO, (b) MXene/Bi_2O_3/Bi_2S_3/ITO, (c) Au/MXene/Bi_2O_3/Bi_2S_3/ITO, (d) EDT/Au/MXene/Bi_2O_3/Bi_2S_3/ITO, (e) P1/EDT/Au/MXene/Bi_2O_3/Bi_2S_3/ITO, (f) P2/P1/EDT/Au/MXene/Bi_2O_3/Bi_2S_3/ITO, and (g) MB/P2/P1/EDT/Au/MXene/Bi_2O_3/Bi_2S_3/ITO.

spherical structure of Bi_2O_3 in the form of lamellar aggregates was shown in Figure 1A. Figure 1B showed a radial flower-like Bi_2S_3 composed of self-assembled nanorods. Figure 1C showed the SEM image of Bi_2O_3/Bi_2S_3 S-4, indicating that Bi_2O_3/Bi_2S_3

https://doi.org/10.1021/acssensors.2c01600
ACS Sens. 2022, 7, 3116−3125

S-4 is a flower-like structure modified as a few nanorods on the surface with a diameter of 4−5 μm. Figure 1D showed the XRD patterns of pure Bi_2O_3, pure Bi_2S_3, and the Bi_2O_3/Bi_2S_3 S-4 heterojunction. All labeled diffraction peaks of Bi_2O_3 and Bi_2S_3 corresponded to cubic Bi_2O_3 (JCPDS No. 76−2478) and orthorhombic Bi_2S_3 (JCPDS No. 84−0279), respectively.[25] The intensity of the diffraction peak of Bi_2O_3 was weak, demonstrating the low crystallinity of Bi_2O_3, because it is difficult to obtain Bi_2O_3 with high crystallinity without further annealing.[48] For Bi_2O_3/Bi_2S_3 S-4, both diffraction peaks of Bi_2O_3 and Bi_2S_3 appeared, indicating the successful preparation of Bi_2O_3/Bi_2S_3 composite. The effect of thiourea amount on the preparation of Bi_2O_3/Bi_2S_3 that was studied was presented in Figure 1E. With the introduction of thiourea, the diffraction peak of Bi_2O_3 still existed, but a new diffraction signal of Bi_2S_3 with an orthogonal crystal phase appeared.[48] With the increase of thiourea content, the diffraction peak intensity of the Bi_2S_3 phase gradually increased, while that of the Bi_2O_3 phase gradually decreased. In addition, the HRTEM images of the Bi_2O_3/Bi_2S_3 S-4 heterojunction (Figure 1F) displayed significantly both groups of crystal lattice stripes. Sequenced crystal lattice stripes spaced at 0.557 nm correspond well to the (200) plane of rhombic Bi_2S_3, while lattice stripes spaced at 0.315 nm correspond in a good way to the (111) plane of cubic Bi_2O_3.

The successful preparation of the Bi_2O_3/Bi_2S_3 heterojunction was further demonstrated by X-ray photoelectron spectroscopy (XPS) investigations. The XPS survey spectrum of Bi_2O_3/Bi_2S_3 was shown in Figure 1G, demonstrating the two peaks occurred at 159.5 and 164.8 eV attributed to the Bi $4f_{7/2}$ and Bi $4f_{5/2}$ of Bi^{3+} in the high-resolution XPS spectra of Bi_2O_3/Bi_2S_3 (Figure 1H).[49] In particular, the O 1s peak was separated into two peaks at 529.8 and 531.2 eV (Figure 1I), with the lattice oxygen and surface hydroxyl groups corresponding to the Bi−O species, respectively.[49] The existence of chiral separation between the peaks of S $2p_{3/2}$ (163.3 eV) and S $2p_{1/2}$ (164.3 eV) (Figure 1J) indicated that there was S^{2-} in Bi_2O_3/Bi_2S_3 nanoflowers, which was consistent with previous studies.[50] The SEM image of MXene with a lamellar structure of loose layers was shown in Figure 1K. XRD patterns corresponding to MXene with the characteristic diffraction peaks at (002), (004), (104), and (105) crystal planes corresponding to 9.2°, 12.9°, 39.0°, and 41.9°, depending on the composition of Ti_3AlC_2 was demonstrated in Figure 1L.[51] The 39.0° (104) diffraction peak disappeared by etching, indicating the exhaustive removal of the Al element from Ti_3AlC_2. In addition, the intensity of the Ti_3C_2 diffraction peak was weaker compared with Ti_3AlC_2, which proves that Ti_3C_2 had a thinner layer structure.

Enhancing Mechanism of Optical Activity of Bi_2O_3/Bi_2S_3 by MXene. The effect of MXene and Bi_2S_3 on the PEC response of Bi_2O_3 was investigated in 0.1 M Tris-HCl solution containing 0.1 M MB (pH = 7.4). In this regard, five varieties of ITO electrodes, Bi_2O_3/ITO, Bi_2S_3/ITO, MXene/ITO, Bi_2O_3/Bi_2S_3/ITO, and MXene/Bi_2O_3/Bi_2S_3/ITO, were fabricated. Figure 2A showed that MXene/ITO presented no PEC response (curve a) with the applied potential of 0 V. Bi_2O_3/ITO (curve b) and Bi_2S_3/ITO (curve c) showed weak PEC response. However, Bi_2O_3/Bi_2S_3/ITO exhibited a significantly strong PEC response (curve d), suggesting that the addition of Bi_2S_3 dramatically enhanced the PEC activity of Bi_2O_3. It was attributed to the heterojunction structure formed between Bi_2O_3 and Bi_2S_3, which efficiently suppressed the recombination of photogenerated electron−hole pairs and improved the mobility of photogenerated electrons. When MXene was further modified on Bi_2O_3/Bi_2S_3/ITO, the photocurrent was obviously enhanced (curve e), which demonstrated that MXene further enhanced the photoelectron−hole pair separations and expedited the transmission of photogenerated electrons. In this regard, a comparison study was established to further explore the effect of MB on the photosensitive products. This means that the PEC response of MXene/Bi_2O_3/Bi_2S_3/ITO in 0.1 M Tris−HCl (pH = 7.4) solution was studied. As shown in Figure S1, the photocurrent of MXene/Bi_2O_3/Bi_2S_3/ITO decreased dramatically from 515 nA to 190 nA when there was no MB in the detection buffer. This fully demonstrated the sensitization of the photoactive material by MB.

The mechanism of PEC signal improvement was investigated by EIS, PL, UV−vis DRS, and Mott−Schottky experiments. First, through the EIS analysis of the carrier transformation in the process, the arc length radius was proportional to the charge division resistance (R_{et}) of the interface. In general, the shorter the semicircular arc of the EIS spectrum, the lower the interfacial resistance and the faster the electron transfer process.[52] As shown in Figure 2B, Bi_2S_3 (curve a) and Bi_2O_3 (curve b) presented a large semicircle diameter, indicating high interface charge transfer resistance. When Bi_2O_3 was compounded with Bi_2S_3, the value of R_{et} was significantly reduced by the formatting of the heterojunction structure, and this benefited the separation and transfer of the photoexcited carriers (curve c). It is well-known that MXene has good electrical conductivity due to its unique metal-like qualities; thus its resistance value was smaller (curve d). When Bi_2O_3/Bi_2S_3 was combined with MXene, the R_{et} value was significantly reduced (curve e), demonstrating that MXene increased the electron transport rate noticeably and decreased the photoelectron−hole pair complexes, which resulted in an improved photocurrent signal.

PL intensity is closely related to the photoexcited electron−hole complexation, and the lower the PL intensity, the weaker the electron−hole recombination.[51] Moreover, the lower intensity of the PL peak indicates a slower recombination of electrons and holes. As presented in Figure 2C, the PL signals of pure Bi_2O_3 (curve a) and Bi_2S_3 (curve b) were very obvious, and the intensity of the PL spectra of Bi_2O_3/Bi_2S_3 (curve c) was significantly weakened. The results indicated that the construction of the Bi_2O_3/Bi_2S_3 heterojunction effectively inhibited the recombination of photoexcited electron−hole pairs. With the addition of MXene, the PL intensity of MXene/Bi_2O_3/Bi_2S_3 (curve d) further decreased because MXene with good conductivity provided a fast channel for the transfer and migration of photogenerated carriers in the composite. Therefore, the formation of the energy band matching structure of Bi_2O_3/Bi_2S_3 and MXene can not only effectively suppress the recombination of photogenerated carriers but also prolong the lifetime of photogenerated electrons, thus effectively improving the photoelectrochemical activity. The UV−vis DRS of Bi_2O_3, Bi_2S_3, MXene, Bi_2O_3/Bi_2S_3, and MXene/Bi_2O_3/Bi_2S_3 were measured. As shown in Figure 2D, the absorption of Bi_2O_3 was weak (curve a), especially in the visible range. Bi_2S_3 presented full absorption in the visible range (curve b). Compared with pure Bi_2O_3 (curve a) and pure Bi_2S_3 (curve b), Bi_2O_3/Bi_2S_3 (curve c) showed increased absorption in the visible region. MXene also illustrated full spectrum light absorption in the whole spectral range (curve

https://doi.org/10.1021/acssensors.2c01600
ACS Sens. 2022, 7, 3116−3125

d). When Bi_2O_3/Bi_2S_3 was further combined with MXene, MXene/Bi_2O_3/Bi_2S_3 showed stronger light-trapping ability, verifying the positive effect of black MXene in enhancing the light absorption in favor of photocurrent enhancement.

Mott−Schottky curves of the electrochemistry of Bi_2O_3, Bi_2S_3, and MXene have been investigated first in advance for the purpose of understanding that energy band information on the nanomaterials prepared. The electrochemical Mott−Schottky slopes of Bi_2O_3, Bi_2S_3, and MXene were both positive, demonstrating that they were *n*-type semiconductors, at the intersection of Figure 2E, F, and G. From the intersection of the tangent and transverse coordinates, the flat-band potentials (E_f) of Bi_2O_3, Bi_2S_3, and MXene are −1.92, −0.22, and 0.46 V (relative to the saturated glycury electrode, SCE), respectively. Depending on equation of $E_{NHE} = E_{SCE} + 0.24$,[53] the E_f values for Bi_2O_3, Bi_2S_3, and MXene were −1.68, 0.02, and 0.7 eV (with respect to the standard hydrogen electrode, NHE), respectively.[54,55] The conduction band potential (E_{CB}) approached the flat band potential to the *n*-type semiconductor. The E_{CB} values for Bi_2O_3 and Bi_2S_3 were calculated on the basis of the equation of $E_{CB} = E_{fb} - 0.2$;[56] the E_{CB} values of Bi_2O_3 and Bi_2S_3 are −1.88 and −0.18 eV (vs NHE), respectively. Furthermore, the band gap widths of Bi_2O_3 and Bi_2S_3 were found to be 3.63 and 1.47 eV (vs NHE), respectively,[25,55] by UV−vis DRS, as shown in Figure 2H and I. The E_{VB} of Bi_2O_3 and Bi_2S_3 were calculated to be 1.75 and 1.29 eV (vs NHE), respectively, according to the equation of $E_{CB} = E_{VB} - E_g$.[57] With its wide band gap, Bi_2O_3 was difficult to be excited by visible light. It was a requirement to combine Bi_2O_3 with other semiconductor materials with narrower band gaps to construct heterojunctions to improve its photoelectric activity. With the narrow band gap, Bi_2S_3 was readily excited by visible light to generate photogenerated electron and hole pairs. With its metal-like nature, MXene provided suitable Fermi energy levels to form band-matched structures with photoactive materials.[32] When excited by visible light, the difficult-to-excite Bi_2O_3 can be excited by visible light, because it forms a heterojunction with Bi_2S_3 and the band gap is reduced, and the photogenerated electrons of Bi_2O_3/Bi_2S_3 migrate from the conducting band to the flat band of MXene and then are absorbed by the electrode, generating the intense photocurrent response. According to the analysis above, probable mechanisms of PEC signal strengthening were given in Figure 2J.

Evaluation of Detection Feasibility. The optical response of different electrodes was studied in 0.1 M Tris-HCl (pH = 7.4) solution to verify the suitability of the biosensor for the TET1 protein detection. The enhanced photocurrent response exhibited by MXene/Bi_2O_3/Bi_2S_3/ITO (curve b) in comparison with the bare ITO electrode (curve a), as shown in Figure 2L, was a result of the good energy band matching structure between MXene and Bi_2O_3/Bi_2S_3, which led to the excellent photoelectric activity. When AuNPs were modified onto the MXene/Bi_2O_3/Bi_2S_3/ITO surface, the photocurrent signal decreases (curve c). It was ascribed to the negative charge on the AuNPs surface and the small size of AuNPs with insulating properties, inhibiting the transfer rate of photogenerated electron, resulting in a lower photocurrent signal.[58] Upon modification of the electrode surface by EDT, which was due to the poor charge conversion of organic small molecules, the photocurrent signal is further reduced (curve d).[46] When the 5hmC-DNA and DNA 1 were gradually assembled, the photocurrent signal decreased due to the spatial site resistance effect and electrostatic repulsion effect of biomolecules which reduced the electron transfer rate (curve e and f, respectively). Eventually, the MB was markedly enlarged in photocurrent when incubated on the modified electrode (curve g). A large amount of MB was inserted into the G-wire by electrostatic attraction, which achieved effective sensitization to MXene/Bi_2O_3/Bi_2S_3. Based on the photocurrent response change, the detection feasibility was confirmed.

Optimization of Detection Conditions. See Supporting Information.

Detection Performance for TET1 Protein. Modification of the PEC signal of the sensor fabricated in relation to the concentration of TET1 protein was measured in relation to the amount of MB. The quantitative performance of the PEC sensor for TET1 protein analysis was assessed by testing various concentrations of TET1 protein under optimal conditions of experimentation and according to the proposed PEC strategy. Progressively, the signal of the photocurrent was enhanced with the TET1 protein concentration, as shown in Figure 3A. In the range of 0.1−10 μg/mL, there was a good

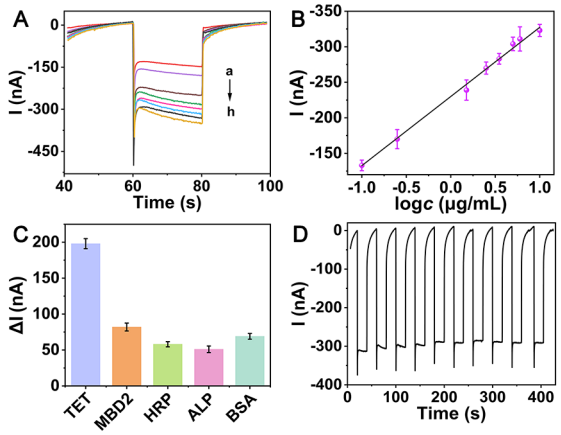

Figure 3. (A) Response of PEC of biosensor from different concenrations of TET1 protein. (a−h) 0.1, 0.25, 1.5, 2.5, 3.5, 5, 6, and 10 μg/mL. (B) Linear relationship between the photocurrent and the logarithm value of TET1 protein concentration. Direct linear relationship between photocurrent and concentration of TET1 protein against the value. (C) Variation of PEC response of biosensor prepared with different proteins. Protein concentration is 2.5 μg/mL. (D) Time-based response of photocurrent for a biosensor with the light on−off cycles. TET1 concentration is 2.5 μg/mL.

linear relationship between the PEC signal and the logarithm of TET1 protein concentration (Figure 3B). The linear equation was I(nA) = −97.3 log c (μg/mL) − 230, with a correlation coefficient of 0.997 and a detection limit of 0.014 μg/mL (3σ). Compared with the existing detection methods (Table 1), this biosensor showed a wide detection range and a low detection limit.

To evaluate the detection selectivity of the prepared PEC biosensor platform for TET1 protein, several proteins were employed to prepare the biosensor, such as MBD2, HRP, ALP, and BSA. The electrode was prepared according to the procedure, except that TET1 protein was replaced by another protein. To perform it, the protein concentration was 2.5 μg/mL. As illustrated in Figure 3C, the PEC change for the TET1 protein was greatly higher than that for other proteins, indicating the high selectivity of the developed method for TET1 protein detection.

https://doi.org/10.1021/acssensors.2c01600
ACS Sens. 2022, 7, 3116−3125

Table 1. Analysis of the Detection Property of the PEC Biosensor by Comparison with Other TET1 Protein Detection Methods

Target	Methods	Linear range (μg/mL)	Detection limit (μg/mL)	Ref
TET1	FL	10.5−52.5	5.4	10
TET1	LC-MS	10−30	\	11
TET1	ECL	1−10	0.37	12
TET1	EC	4.2−21	0.98	59
TET1	PEC	0.1−10	0.014	This work

In addition, the repeatability of the constructed biosensor platform was evaluated by testing the switching light period of the prepared electrode, in which the electrode was prepared with 2.5 μg/mL of TET1 protein. As shown in Figure 3D, the photocurrent response showed negligible changes after 10 cycles, and the relative standard deviation (RSD) was 1.61%, which indicated that the biosensor had good stability.

Inhibition on TET1 Activity. TET1 protein is a DNA demethylation protein, and its abnormal activity is often associated with the occurrence and development of diseases.[59] Thus, TET1 protein can be used as a therapeutic target molecule to screen for drugs that can inhibit its activity, providing therapeutic drugs for diseases induced by its abnormal activity. Thus, to evaluate the applicability of the developed method, the inhibitor screening experiment was performed, where a known inhibitor of Bobcat339 for TET1 protein was employed. As shown in Figure 4A, by increasing

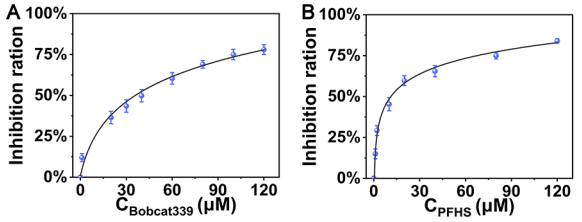

Figure 4. Effects of inhibitor (A) and environmental pollutant (B) on TET activity. Bobcat339 (A) and Perfluorohexanesulfonate (B).

Bobcat339 concentration from 1 to 120 μM, the inhibition efficiency toward TET1 protein increased gradually. The IC_{50} value was calculated to be 36.1 μM, which was close to the previous report.[60] This result demonstrated that the developed method could be applied in the field of drug screening for TET1 protein-related diseases. The application of the developed method in the field of assessment of the toxicological effects of environmental pollutants has also been evaluated. To perform it, a typical environmental pollutant of perfluorohexanesulfonate (PFHS) was employed, and its influence on TET1 protein activity was investigated. As illustrated in Figure 4B, PFHS inhibited TET1 protein activity with the IC_{50} value of 11.2 μM. Thus, the TET1 protein might be acting as a new biomarker in the field of evaluation of toxicological effects of environmental pollutants, and the developed method might be acting as a new assessment technique for evaluation of toxicological effects of environmental pollutants.

CONCLUSION

In summary, a novel PEC biosensor was constructed for TET1 protein detection by taking advantage of the catalytic oxidation property of TET1 protein toward 5mC. With the heterojunction structure of Bi_2O_3/Bi_2S_3 and the matched energy band of MXene with Bi_2O_3/Bi_2S_3, the significant increase in the photoactivity of MXene/Bi_2O_3/Bi_2S_3 also enhanced the sensitivity of the assay. In addition, DNA Walker triggering nicking enzyme-assisted single-stranded DNA release, and the MB sensitization strategy further improved the detection sensitivity. Based on the specific oxidation ability of the TET1 protein for 5mC to generate 5hmC, the detection selectivity was realized. With excellent selectivity and stability, the proposed PEC strategy can be expected to be a suitable low-cost detection tool for TET1 protein and develop new avenues for the sensitive identification of additional biomarkers used for disease diagnosis.

ASSOCIATED CONTENT

Supporting Information

The Supporting Information is available free of charge at https://pubs.acs.org/doi/10.1021/acssensors.2c01600.

Materials and instruments; preparation of Bi_2O_3/Bi_2S_3 materials; synthesis of MXene; the Nb.BvCI enzyme-assisted signal amplification; biosensor fabrication; inhibition assay; PEC response of MXene/Bi_2O_3/Bi_2S_3 in different detection solutions; optimization of detection conditions (PDF)

AUTHOR INFORMATION

Corresponding Authors

Yunlei Zhou − *College of Chemistry and Material Science, Key Laboratory of Agricultural Film Application of Ministry of Agriculture and Rural Affairs, Food Safety Analysis and Test Engineering Technology Research Center of Shandong Province, Shandong Agricultural University, 271018 Taian, Shandong, People's Republic of China*; Email: zhyl@sdau.edu.cn

Huanshun Yin − *College of Chemistry and Material Science, Key Laboratory of Agricultural Film Application of Ministry of Agriculture and Rural Affairs, Food Safety Analysis and Test Engineering Technology Research Center of Shandong Province, Shandong Agricultural University, 271018 Taian, Shandong, People's Republic of China*; orcid.org/0000-0002-5022-0314; Email: yinhs@sdau.edu.cn

Authors

Yulin Zheng − *College of Chemistry and Material Science, Key Laboratory of Agricultural Film Application of Ministry of Agriculture and Rural Affairs, Food Safety Analysis and Test Engineering Technology Research Center of Shandong Province, Shandong Agricultural University, 271018 Taian, Shandong, People's Republic of China*

Xiaoting Cui − *College of Chemistry and Material Science, Key Laboratory of Agricultural Film Application of Ministry of Agriculture and Rural Affairs, Food Safety Analysis and Test Engineering Technology Research Center of Shandong Province, Shandong Agricultural University, 271018 Taian, Shandong, People's Republic of China*

Haowei Zhang − *College of Chemistry and Material Science, Key Laboratory of Agricultural Film Application of Ministry of Agriculture and Rural Affairs, Food Safety Analysis and Test Engineering Technology Research Center of Shandong Province, Shandong Agricultural University, 271018 Taian, Shandong, People's Republic of China*

https://doi.org/10.1021/acssensors.2c01600
ACS Sens. 2022, 7, 3116−3125

Lulu Cao − *College of Chemistry and Material Science, Key Laboratory of Agricultural Film Application of Ministry of Agriculture and Rural Affairs, Food Safety Analysis and Test Engineering Technology Research Center of Shandong Province, Shandong Agricultural University, 271018 Taian, Shandong, People's Republic of China*

Lanlan Gao − *College of Chemistry and Material Science, Key Laboratory of Agricultural Film Application of Ministry of Agriculture and Rural Affairs, Food Safety Analysis and Test Engineering Technology Research Center of Shandong Province, Shandong Agricultural University, 271018 Taian, Shandong, People's Republic of China*

Shiyun Ai − *College of Chemistry and Material Science, Key Laboratory of Agricultural Film Application of Ministry of Agriculture and Rural Affairs, Food Safety Analysis and Test Engineering Technology Research Center of Shandong Province, Shandong Agricultural University, 271018 Taian, Shandong, People's Republic of China;* orcid.org/0000-0003-0449-3677

Complete contact information is available at: https://pubs.acs.org/10.1021/acssensors.2c01600

Notes

The authors declare no competing financial interest.

■ ACKNOWLEDGMENTS

This work was supported by the Outstanding Youth Innovation Team of University in Shandong Province (2019KJC019), the Key Research and Development (Public Welfare) Project of Shandong Province (2019GSF107023), the National Natural Science Foundation of China (41977345, 41807484, 42077363).

■ REFERENCES

(1) Zhang, H.; Lang, Z.; Zhu, J. K. Dynamics and function of DNA methylation in plants. *Nat. Rev. Mol. Cell Biol.* **2018**, *19*, 489−506.

(2) Zhou, Y.; Yin, H.; Zhao, W.-W.; Ai, S. Electrochemical, electrochemiluminescent and photoelectrochemical bioanalysis of epigenetic modifiers: A comprehensive review. *Coord. Chem. Rev.* **2020**, *424*, 213519.

(3) Hu, L.; Lu, J.; Cheng, J.; Rao, Q.; Li, Z.; Hou, H.; Lou, Z.; Zhang, L.; Li, W.; Gong, W.; Liu, M.; Sun, C.; Yin, X.; Li, J.; Tan, X.; Wang, P.; Wang, Y.; Fang, D.; Cui, Q.; Yang, P.; et al. Structural insight into substrate preference for TET-mediated oxidation. *Nature* **2015**, *527*, 118−122.

(4) Ito, S.; Shen, L.; Dai, Q.; Wu, S. C.; Collins, L. B.; Swenberg, J. A.; He, C.; Zhang, Y. Tet Proteins Can Convert 5-Methylcytosine to 5-Formylcytosine and 5-Carboxylcytosine. *Science* **2011**, *333*, 1300.

(5) Gao, F.; Xia, Y.; Wang, J.; Luo, H.; Gao, Z.; Han, X.; Zhang, J.; Huang, X.; Yao, Y.; Lu, H.; Yi, N.; Zhou, B.; Lin, Z.; Wen, B.; Zhang, X.; Yang, H.; Wang, J. Integrated detection of both 5-mC and 5-hmC by high-throughput tag sequencing technology highlights methylation reprogramming of bivalent genes during cellular differentiation. *Epigenetics* **2013**, *8*, 421−430.

(6) Luo, X.; Jiang, L.; Kang, T.; Xing, Y.; Zheng, E.; Wu, P.; Cai, C.; Yu, Q. Label-Free Raman Observation of TET1 Protein-Mediated Epigenetic Alterations in DNA. *Anal. Chem.* **2019**, *91*, 7304−7312.

(7) Pfeifer, G. P; Kadam, S.; Jin, S.-G. 5-hydroxymethylcytosine and its potential roles in development and cancer. *Epigenetics & Chromatin* **2013**, *6*, 10.

(8) Joshi, K.; Liu, S.; Breslin, S. J. P.; Zhang, J. Mechanisms that regulate the activities of TET proteins. *Cell. Mol. Life. Sci.* **2022**, *79*, 363.

(9) Shen, L.; Zhang, Y. Enzymatic analysis of Tet proteins: key enzymes in the metabolism of DNA methylation. *Meth. Enzymol.* **2012**, *512*, 93−105.

(10) Chen, X.; Cheng, Y.; Wang, Y.; Tang, J.; Wang, F.; Chen, Z. Fluorescence assay based on the thioflavin T-induced conformation switch of G-quadruplexes for TET1 detection. *Analyst* **2021**, *146*, 2126−2130.

(11) Liu, M. Y.; DeNizio, J. E.; Kohli, R. M. Quantification of Oxidized 5-Methylcytosine Bases and TET Enzyme Activity. *Meth. Enzymol.* **2016**, *573*, 365−385.

(12) Jiang, W.; Yin, H.; Zhou, Y.; Duan, J.; Li, H.; Wang, M.; Waterhouse, G. I. N.; Ai, S. A novel electrochemiluminescence biosensor for the detection of 5-methylcytosine, TET 1 protein and β-glucosyltransferase activities based on gold nanoclusters-H_2O_2 system. *Sens. Actuators B Chem.* **2018**, *274*, 144−151.

(13) Sui, C.; Wang, T.; Zhou, Y.; Yin, H.; Meng, X.; Zhang, S.; Waterhouse, G. I. N.; Xu, Q.; Zhuge, Y.; Ai, S. Photoelectrochemical biosensor for hydroxymethylated DNA detection and T4-beta-glucosyltransferase activity assay based on WS_2 nanosheets and carbon dots. *Biosens. Bioelectron.* **2019**, *127*, 38−44.

(14) Li, F.; Zhou, Y.; Yin, H.; Ai, S. Recent advances on signal amplification strategies in photoelectrochemical sensing of microRNAs. *Biosens. Bioelectron.* **2020**, *166*, 112476.

(15) Chen, Y.; Zhou, Y.; Yin, H. Recent advances in biosensor for histone acetyltransferase detection. *Biosens. Bioelectron.* **2021**, *175*, 112880.

(16) Zhang, X. Y.; Han, L.; Dan Yu, L.; Wang, X. H.; Ling, Y.; Li, N. B.; Luo, H. Q. Crystal Violet-Sensitized Direct Z-Scheme Heterojunction Coupled with a G-Wire Superstructure for Photoelectrochemical Sensing of Uracil-DNA Glycosylase. *ACS Appl. Mater. Interfaces* **2021**, *13*, 15881−15889.

(17) Shinde, N. M.; Shinde, P. V.; Mane, R. S.; Ho Kim, K. Solution-method processed Bi-type nanoelectrode materials for supercapacitor applications: A review. *Renew. Sust. Energy Rev.* **2021**, *135*, 110084.

(18) Ling, C. D.; Withers, R. L.; Schmid, S.; Thompson, J. G. A Review of Bismuth-Rich Binary Oxides in the Systems Bi_2O_3-Nb_2O_5, Bi_2O_3-Ta_2O_5, Bi_2O_3-MoO_3, and Bi_2O_3-WO_3. *J. Solid. State. Chem.* **1998**, *137*, 42−61.

(19) Yan, Q.; Xie, X.; Liu, Y.; Wang, S.; Zhang, M.; Chen, Y.; Si, Y. Constructing a new Z-scheme multi-heterojunction photocataslyts Ag-AgI/BiOI-Bi_2O_3 with enhanced photocatalytic activity. *J. Hazard. Mater.* **2019**, *371*, 304−315.

(20) Chen, L.; He, J.; Yuan, Q.; Liu, Y.; Au, C.-T.; Yin, S.-F. Environmentally benign synthesis of branched Bi_2O_3-Bi_2S_3 photocatalysts by an etching and re-growth method. *J. Mater. Chem. A* **2015**, *3*, 1096−1102.

(21) Wang, S.; Li, X.; Chen, Y.; Cai, X.; Yao, H.; Gao, W.; Zheng, Y.; An, X.; Shi, J.; Chen, H. A Facile One-Pot Synthesis of a Two-Dimensional MoS_2/Bi_2S_3 Composite Theranostic Nanosystem for Multi-Modality Tumor Imaging and Therapy. *Adv. Mater.* **2015**, *27*, 2775−2782.

(22) Zhu, Z.; Iyemperumal, S. K.; Kushnir, K.; Carl, A. D.; Zhou, L.; Brodeur, D. R.; Grimm, R. L.; Titova, L. V.; Deskins, N. A.; Rao, P. M. Enhancing the solar energy conversion efficiency of solution-deposited Bi_2S_3 thin films by annealing in sulfur vapor at elevated temperature. *Sustain. Energy Fuels* **2017**, *1*, 2134−2144.

(23) Whittaker-Brooks, L.; Gao, J.; Hailey, A. K.; Thomas, C. R.; Yao, N.; Loo, Y.-L. Bi_2S_3 nanowire networks as electron acceptor layers in solution-processed hybrid solar cells. *J. Mater. Chem. C* **2015**, *3*, 2686−2692.

(24) Low, J.; Yu, J.; Jaroniec, M.; Wageh, S.; Al-Ghamdi, A. A. Heterojunction Photocatalysts. *Adv. Mater.* **2017**, *29*, 1601694.

(25) Sang, Y.; Cao, X.; Dai, G.; Wang, L.; Peng, Y.; Geng, B. Facile one-pot synthesis of novel hierarchical Bi_2O_3/Bi_2S_3 nanoflower photocatalyst with intrinsic p−n junction for efficient photocatalytic removals of RhB and Cr(VI). *J. Hazard. Mater.* **2020**, *381*, 120942.

(26) Lukatskaya, M. R.; Mashtalir, O.; Ren, C. E.; Dall'Agnese, Y.; Rozier, P.; Taberna, P. L.; Naguib, M.; Simon, P.; Barsoum, M. W.;

Gogotsi, Y. Cation Intercalation and High Volumetric Capacitance of Two-Dimensional Titanium Carbide. *Science* **2013**, *341*, 1502.
(27) Naguib, M.; Halim, J.; Lu, J.; Cook, K. M.; Hultman, L.; Gogotsi, Y.; Barsoum, M. W. New two-dimensional niobium and vanadium carbides as promising materials for Li-ion batteries. *J. Am. Chem. Soc.* **2013**, *135*, 15966−15969.
(28) Bai, X.; Guan, J. MXenes for electrocatalysis applications: Modification and hybridization. *Chin. J. Catal.* **2022**, *43*, 2057−2090.
(29) Wang, Q.; Xiao, X.; Hu, X.; Huang, L.; Li, T.; Yang, M. Molecularly imprinted electrochemical sensor for ascorbic acid determination based on MXene modified electrode. *Mater. Lett.* **2021**, *285*, 129158.
(30) Alwarappan, S.; Nesakumar, N.; Sun, D.; Hu, T. Y.; Li, C. Z. 2D metal carbides and nitrides (MXenes) for sensors and biosensors. *Biosens. Bioelectron.* **2022**, *205*, 113943.
(31) Ren, T.; Huang, H.; Li, N.; Chen, D.; Xu, Q.; Li, H.; He, J.; Lu, J. 3D hollow MXene@$ZnIn_2S_4$ heterojunction with rich zinc vacancies for highly efficient visible-light photocatalytic reduction. *J. Colloid Interface Sci.* **2021**, *598*, 398−408.
(32) Zhao, D.; Cai, C. Preparation of Bi_2MoO_6/Ti_3C_2 MXene heterojunction photocatalysts for fast tetracycline degradation and Cr(VI) reduction. *Inorg. Chem. Front.* **2020**, *7*, 2799−2808.
(33) Chen, S.; Liu, R.; Kuai, Z.; Li, X.; Lian, S.; Jiang, D.; Tang, J.; Li, L.; Wu, R.; Peng, C. Facile synthesis of a novel $BaSnO_3$/MXene nanocomposite by electrostatic self-assembly for efficient photodegradation of 4-nitrophenol. *Environ. Res.* **2022**, *204*, 111949.
(34) Yang, J.-X.; Yu, W.-B.; Li, C.-F.; Dong, W.-D.; Jiang, L.-Q.; Zhou, N.; Zhuang, Z.-P.; Liu, J.; Hu, Z.-Y.; Zhao, H.; Li, Y.; Chen, L.; Hu, J.; Su, B.-L. PtO nanodots promoting Ti_3C_2 MXene in-situ converted Ti_3C_2/TiO_2 composites for photocatalytic hydrogen production. *Chem. Eng. J.* **2021**, *420*, 129695.
(35) Rasheed, T.; Rasheed, A.; Munir, S.; Ajmal, S.; Muhammad Shahzad, Z.; Alsafari, I. A.; Ragab, S. A.; Agboola, P. O.; Shakir, I. A cost-effective approach to synthesize $NiFe_2O_4$/MXene heterostructures for enhanced photodegradation performance and anti-bacterial activity. *Adv. Powder Technol.* **2021**, *32*, 2248−2257.
(36) Alsafari, I. A. Synthesis of CuO/MXene nanocomposite to study its photocatalytic and antibacterial properties. *Ceram. Int.* **2022**, *48*, 10960.
(37) Kou, B. B.; Zhang, L.; Xie, H.; Wang, D.; Yuan, Y. L.; Chai, Y. Q.; Yuan, R. DNA Enzyme-Decorated DNA Nanoladders as Enhancer for Peptide Cleavage-Based Electrochemical Biosensor. *ACS Appl. Mater. Interfaces* **2016**, *8*, 22869−22874.
(38) Xiong, E.; Yan, X.; Zhang, X.; Li, Y.; Yang, R.; Meng, L.; Chen, J. A new photoelectrochemical biosensor for ultrasensitive determination of nucleic acids based on a three-stage cascade signal amplification strategy. *Analyst* **2018**, *143*, 2799−2806.
(39) Cao, J. T.; Lv, J. L.; Liao, X. J.; Ma, S. H.; Liu, Y. M. A membraneless self-powered photoelectrochemical biosensor based on $Bi_2S_3/BiPO_4$ heterojunction photoanode coupling with redox cycling signal amplification strategy. *Biosens. Bioelectron.* **2022**, *195*, 113651.
(40) Zhang, S.; Li, R.; Liu, X.; Yang, L.; Lu, Q.; Liu, M.; Li, H.; Zhang, Y.; Yao, S. A novel multiple signal amplifying immunosensor based on the strategy of in situ-produced electroactive substance by ALP and carbon-based Ag-Au bimetallic as the catalyst and signal enhancer. *Biosens. Bioelectron.* **2017**, *92*, 457−464.
(41) Wang, H.; Li, M.; Zheng, Y.; Hu, T.; Chai, Y.; Yuan, R. An ultrasensitive photoelectrochemical biosensor based on $[Ru(dcbpy)_2dppz]^{2+}$/Rose Bengal dyes co-sensitized fullerene for DNA detection. *Biosens. Bioelectron.* **2018**, *120*, 71−76.
(42) Zeng, Z.; Tang, J.; Zhang, M.; Pu, S.; Tang, D. Ultrasensitive zero-background photoelectrochemical biosensor for analysis of organophosphorus pesticide based on in situ formation of DNA-templated Ag_2S photoactive materials. *Anal. Bioanal. Chem.* **2021**, *413*, 6279−6288.
(43) Chang, J.; Lv, W.; Wu, J.; Li, H.; Li, F. Simultaneous photoelectrochemical detection of dual microRNAs by capturing CdS quantum dots and methylene blue based on target-initiated strand displaced amplification. *Chin. Chem. Lett.* **2021**, *32*, 775−778.
(44) Zhu, M.; Zhong, X.; Deng, H.; Huang, L.; Yuan, R.; Yuan, Y. Dependent signal quenching and enhancing triggered by bipedal DNA walker for ultrasensitive photoelectrochemical biosensor. *Biosens. Bioelectron.* **2019**, *143*, 111618.
(45) Wang, Q.; Yin, H.; Ding, J.; Zhou, Y.; Ai, S. WS_2/Bi/BiOBr Nanostructures for Photoelectrochemical Sensing of 5-Formyluracil-2′-deoxyuridine-5′-triphosphate through Hemin/G-Quadruplex Double Signal Amplification. *ACS Appl. Nano Mater.* **2021**, *4*, 8998−9007.
(46) Long, D.; Li, M.; Wang, H.; Wang, H.; Chai, Y.; Yuan, R. A photoelectrochemical biosensor based on fullerene with methylene blue as a sensitizer for ultrasensitive DNA detection. *Biosens. Bioelectron.* **2019**, *142*, 111579.
(47) Ren, W.; Zhang, Y.; Chen, H. G.; Gao, Z. F.; Li, N. B.; Luo, H. Q. Ultrasensitive Label-Free Resonance Rayleigh Scattering Aptasensor for Hg^{2+} Using Hg^{2+}-Triggered Exonuclease III-Assisted Target Recycling and Growth of G-Wires for Signal Amplification. *Anal. Chem.* **2016**, *88*, 1385−1390.
(48) Deng, Z.; Liu, T.; Chen, T.; Jiang, J.; Yang, W.; Guo, J.; Zhao, J.; Wang, H.; Gao, L. Enhanced Electrochemical Performances of Bi_2O_3/rGO Nanocomposite via Chemical Bonding as Anode Materials for Lithium Ion Batteries. *ACS Appl. Mater. Interfaces* **2017**, *9*, 12469−12477.
(49) Mi, Y.; Li, H.; Zhang, Y.; Zhang, R.; Hou, W. One-pot synthesis of belt-like Bi_2S_3/BiOCl hierarchical composites with enhanced visible light photocatalytic activity. *Appl. Surf. Sci.* **2017**, *423*, 1062−1071.
(50) Zhou, C.; Cui, K.; Liu, Y.; Li, L.; Zhang, L.; Hao, S.; Ge, S.; Yu, J. Bi_2S_3@MoS_2 Nanoflowers on Cellulose Fibers Combined with Octahedral CeO_2 for Dual-Mode Microfluidic Paper-Based MiRNA-141 Sensors. *ACS Appl. Mater. Interfaces* **2021**, *13*, 32780−32789.
(51) Zhao, X.; Chen, J.; Zhao, C.; Liu, Y.; Liang, Q.; Zhou, M.; Li, Z.; Zhou, Y. Construction $ZnIn_2S_4/Ti_3C_2$ of 2D/2D heterostructures with enhanced visible light photocatalytic activity: A combined experimental and first-principles DFT study. *Appl. Surf. Sci.* **2021**, *570*, 151183.
(52) Shao, B.; Liu, X.; Liu, Z.; Zeng, G.; Liang, Q.; Liang, C.; Cheng, Y.; Zhang, W.; Liu, Y.; Gong, S. A novel double Z-scheme photocatalyst $Ag_3PO_4/Bi_2S_3/Bi_2O_3$ with enhanced visible-light photocatalytic performance for antibiotic degradation. *Chem. Eng. J.* **2019**, *368*, 730−745.
(53) Ding, J.; Zhou, Y.; Wang, Q.; Ai, S. Photoelectrochemical biosensor for DNA hydroxymethylation detection based on the enhanced photoactivity of in-situ synthesized Bi_4NbO_8Cl@Bi_2S_3 heterojunction. *Biosens. Bioelectron.* **2021**, *194*, 113580.
(54) Zhang, J.; Gao, Y.; Liu, P.; Yan, J.; Zhang, X.; Xing, Y.; Song, W. Charge transfer accelerated by internal electric field of MoS_2 QDs-BiOI *p-n* heterojunction for high performance cathodic PEC aptasensing. *Electrochim. Acta* **2021**, *365*, 137392.
(55) Zheng, Y.; Zhou, Y.; Cui, X.; Yan, H.; Cao, L.; Gao, L.; Yin, H. Investigation of the effect of antibiotics on 5-formylcytosine content in mazie seedling tissues based on photoelectrochemical biosensor. *J. Hazard. Mater.* **2022**, *436*, 129146.
(56) Li, F.; Yin, H.; Chen, Y.; Wang, S.; Li, J.; Zhang, Y.; Li, C.; Ai, S. Preparation of P-g-C_3N_4-WS_2 nanocomposite and its application in photoelectrochemical detection of 5-formylcytosine. *J. Colloid Interface Sci.* **2020**, *561*, 348−357.
(57) Zhang, L.; Li, P.; Feng, L.; Chen, X.; Jiang, J.; Zhang, S.; Zhang, C.; Zhang, A.; Chen, G.; Wang, H. Synergetic Ag_2S and ZnS quantum dots as the sensitizer and recognition probe: A visible light-driven photoelectrochemical sensor for the "signal-on" analysis of mercury (II). *J. Hazard. Mater.* **2020**, *387*, 121715.
(58) Cui, X.; Zhou, Y.; Zheng, Y.; Hu, Y.; Wang, Z.; Gao, L.; Cao, L.; Yin, H.; Ai, S. Investigation the effect of antibiotics on the content of N^6-methyladenosine in rice seedling tissue and heavy metal on FTO activity based on antibody-free photoelectrochemcial biosensor. *Sens. Actuators B Chem.* **2022**, *364*, 131896.
(59) Yu, Z.; Chen, X.; Cheng, Y.; Yang, H.; Wang, F.; Chen, Z. Novel label-free electrochemical strategy for sensitive determination of ten-eleven translocation protein 1. *Anal. Chim. Acta* **2021**, *1146*, 140−145.

https://doi.org/10.1021/acssensors.2c01600
ACS Sens. 2022, 7, 3116−3125

(60) Weirath, N. A.; Hurben, A. K.; Chao, C.; Pujari, S. S.; Cheng, T.; Liu, S.; Tretyakova, N. Y. Small Molecule Inhibitors of TET Dioxygenases: Bobcat339 Activity Is Mediated by Contaminating Copper(II). *ACS Med. Chem. Lett.* **2022**, *13*, 792−798.

https://doi.org/10.1021/acssensors.2c01600
ACS Sens. 2022, 7, 3116−3125